Journal of Renewable Materials

Tech Science Press

DOI: 10.32604/jrm.2022.022458

ARTICLE

Mechanical Properties and Evolution of Microstructure of Cement Stabilized Loess

Kangze Yuan[1], Kui Liu[1,2,*], Guoyang Yi[3] and Bowen Yang[2]

[1]College of Geological Engineering and Geomatics, Chang'an University, Xi'an, China

[2]China Information Industry Engineering Investigation and Research Institute, Xi'an, China

[3]School of Civil Engineering, Chang'an University, Xi'an, China

[*]Corresponding Author: Kui Liu. Email: k_135830@foxmail.com

Received: 10 March 2022 Accepted: 08 April 2022

ABSTRACT

Cement Stabilized Loess (CSL) sample has a long history as a method of improving building foundations. In this paper, the main physical (specific gravity, consistency limit, optimum moisture content, and maximum dry density) and mechanical properties (Unconfined Compressive Strength (UCS) and shear strength parameters) of CSL samples with different cement content were investigated, and the change reasons were explored by mean of SEM test. Meanwhile, quantitative analysis software Image-Pro Plus (IPP) 6.0 was used to characterize the microstructural evolution of pores in compacted loess and CSL sample. As the cement content increased, the specific gravity and optimum water content in the CSL samples increased and the liquid limit and maximum dry density decreased. The plastic limit exhibits an increase followed by a decrease, with the plasticity index changing in the opposite tendency. The UCS and shear strengths of the CSL samples increased with increasing cement content, and the USC and cement content was better fitted using the Asymptotic model under the same curing time. The growth rate of the UCS and shear strength parameters were significantly reduced at cement contents above 2%. The results of Scanning Electron Microscopy (SEM) showed that the structure of the CSL samples was denser and had no obvious inter-aggregate pores. Meanwhile, compared to compacted loess, produced C-S-H gel and ettringite. Quantitative analysis of compacted loess and CSL sample by IPP software. Compared to compacted loess, the average pore diameter and average pore area of the CSL sample decreased from 12.44 μm and 229.04 μm^2 to 8.72 μm and 84.68 μm^2, a reduction of 29.9% and 63.0%, respectively. The pore shape tends to flatten, but there is basically no effect on the pore angle distribution. Finally, a systematic description of the physicochemical reactions occurring during the formation of the CSL sample structure was made, and a schematic diagram of the formation of the CSL sample structure was created.

KEYWORDS

Strength; pores; SEM; structure formation; quantitative analysis

1 Introduction

Loess is special sediment formed during the Quaternary period under arid and semi-arid climatic conditions [1,2]. Its deposits cover 10% of continents in the whole world, especially covering 64×10^4 km^2 in China, mainly in the type region of Shanxi, Shaanxi, Gansu, and Ningxia [3–5].

The typical loess is considered to be an aeolian deposit with an open and meta-stable structure [6]. When water enters the loess structure, under the combined effect of the self-weight and additional pressure of the loess, large and rapid settlements will occur, causing different degrees of deformation and even damage, affecting the structural safety of the building [7–9]. Therefore, loess foundations often need to be reinforced during construction in loess areas, thus reducing the impact on people's livelihoods and economic development [10]. Improving the compaction and strength of foundations by compaction of the original foundation is a common method used today [11,12]. However, the specific characteristics of loess can lead to weak cementation between the particles. It is difficult to meet the standards required by the project by simple compaction methods. Therefore, some scholars have started to add binders to the loess to increase the structural strength. Sodium alginate was added to loess by Zhao et al. [13] to investigate the changes in basic physical parameters and mechanical properties, found that sodium alginate not only changes the basic physical parameters of the loess but also improves the mechanical properties. Iranpour et al. [14] explored the effects of four types of nanomaterials on soil structure, and indicated that the addition of nanomaterials has a significant effect on collapsible soils. Choobbasti et al. [15] examined the influence of nano $CaCO_3$ and fibers as reinforcement on the behavior of the soil was investigated and discovered that the joint use of fibers and nanoparticles resulted in a significant increase in strength. Although many scholars' studies have greatly improved the mechanical behavior of soils [16–19], cement stabilized loess is widely used due to its improved mechanical properties, low environmental impact, and high technical efficiency [20].

Significant studies have been carried out to understand the effect of cement on the mechanical behavior of soil. Zhang et al. [21] identified that the main factor in the increase in shear strength of cement stabilized loess was the improvement in cohesion after remolding and that the sensitivity of the cohesion to the structure was much higher than the friction angle. Ghadakpour et al. [22] demonstrated that the stress-strain behavior of the specimens tended to the expected behavior of overconsolidated soils as the percentage of cement was increased. Dynamic elastic modulus, dynamic deformation, and damping ratio of cement stabilized loess were obtained by Wang et al. [23] and displayed that the dynamic properties of cement stabilized loess were better as the cement ratio increased and no optimum cement proportion. The mechanical properties of cement stabilized loess decrease as the number of freeze-thaw (FT) cycles increased [24,25]. Therefore, the addition of cement has a significant effect on the mechanical properties of the loess. The changes in the mechanical properties of CSL samples and their underlying mechanisms are more complex. To clarify these changes and mechanisms, a series of mechanical tests and microstructural scanning are required to investigate the response of the mechanical properties of CSL samples to the microstructural evolution.

With the development of observation and image processing techniques, scanning electron microscopy (SEM), digital microscopy, and X-ray computed tomography (CT) are widely used to obtain complex information on the internal structure of soils [26–28]. Among them, SEM testing is preferred by scholars due to its advantages of simple sample preparation, high resolution, and wide testing range [29]. However, SEM tests can only provide a few images as results and for qualitative analysis, which is not satisfactory for scientific research criteria. To gain more accurate quantitative parameters of the loess microstructure, image processing of SEM results using IPP software is required [30,31]. IPP software is an image analysis software developed by Media Cybernetics, USA, which combines acquisition, processing, and analysis functions to ensure the identification and extraction of microstructural information from images. Sun et al. [32] used IPP software to quantify the CSL samples and found that the unconfined compressive strength of CSL samples increased significantly as the fractal dimension of the pore area decreased. However, the study did not analyze the pores size of the CSL samples. The variation in pore size of CSL samples was explored by Liu et al. [33], but no statements were made about the evolution of pore shape and angle. Although the microstructural parameters of CSL sample pores

have been studied by some scholars, a systematic analysis of the size, shape, and angle of the pore microstructure is still not sufficient.

Based on the above considerations, in this paper, the main physical and mechanical properties of CSL samples with different cement content were investigated, and the microstructural parameters of the pores are then analyzed quantitatively based on the SEM results to obtain the evolution pattern of the microstructural parameters. The innovative contribution of this study is the systematic analysis of the microstructural parameters of the CSL samples and the explanation of the causes of the structural strength formation of CSL samples in connection with the physicochemical reactions occurring between cement and loess particles.

2 Materials and Methodology

2.1 Raw Materials

The investigated samples were loess from the new district of Yan'an City, China, with a depth of 6.0–7.5 m below the natural surface, and can be classified as Malan loess. Fig. 1 shows the surface morphology of the sampling site. The tested loess samples were light brown silty soil with low plasticity. The main physical properties of the loess were determined through the ASTM [34] standard tests and listed in Table 1. The Portland cement was from Shaanxi, China, and the chemical composition of cement was determined by X-ray diffraction and listed in Table 2.

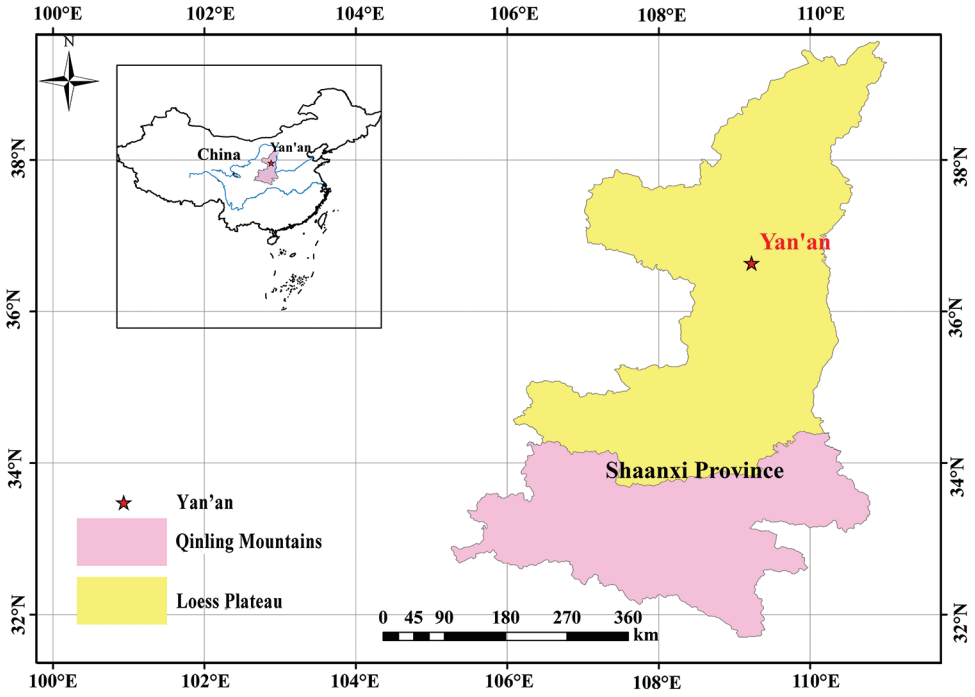

Figure 1: The major occurrence of Loess Plateau in Shaanxi Province and sampling location at the excavation site

Table 1: Main physical properties

Sample measurements	*In situ* density (g/cm^3)	Natural water content (%)	Specific gravity	Plastic limit (ω_P/%)	Liquid limit (ω_L/%)	Plasticity index (Ip)
Loess	1.35	12.35	2.697	14.46	29.32	14.59

Table 2: Cement chemical compositions

	Cement
CaO	65.3
MgO	0.9
Al_2O_3	4.3
Fe_2O_3	5.3
SiO_2	22.9
SO_3	1.3

2.2 Sample Preparation and Test Procedure

For the cement stabilized loess (CSL) samples, the cement (blended ratios at 2%, 4%, 6%, and 8%), and the preparation method was as follows. The loess and cement were crushed until all aggregates were destroyed. The obtained materials were passed through a 0.075 mm sieve and then oven-dried at 105°C for eight hours. Then, the cement, loess, and deionized water were measured by mass according to the predesignated mix ratios. The loess was mixed with lime thoroughly. After that, the amount of deionized water was gradually added to the samples using a spray bottle until the water content was up to the target content. During the addition of water, keep stirring so that the mixture is uniformity. Then strictly sealed with plastic film and placed into a humidity chamber for water homogenization for about 2 days at room temperature. In order to better explained the reason for the change of properties of CSL samples. A blank experiment was also set on loess without adding cement.

The specific gravity of the samples was tested by the density bottle method [35]. The consistency limit was defined by a liquid and plastic limit combined test [36]. The compaction test was carried out under the Unified Soil Classification System [37]. In order to obtain the mechanical properties of the CSL specimens, the samples with different cement contents were static pressed into cylindrical steel molds of Φ 39.1 mm × h 80 mm and Φ 61.8 mm × h 20 mm, respectively, based on the experimental results of the compaction test (optimum water content and compaction coefficient of 95%). They were labeled and placed in a vacuum glass dryer with a diameter of 500 mm and a height of 250 mm. After all, samples were fabricated, the specimens were removed from the molds and were cured in a humid room with a temperature of 25 ± 2°C and relative humidity above 95%, for 7 days, 14 days, and 28 days, respectively. The UCS test was conducted by ASTM D [38]. The samples were placed on an unconfined compressive strength tester with a maximum load capacity of 2.5 kN and compressed at a constant rate of 0.1 mm/min. A strain-controlled direct shear apparatus was used to apply four different vertical pressures to CSL samples [39]. The vertical pressures were 50, 100, 150, 200 kPa, and the shear rate was 0.8~1.2 mm/min to reduce the loss of soil samples within 3~5 min. At each pressure level, the shear strength of the sample reached the peak strength, and for those samples without significant peaks, a strain-hardening stress-strain curve corresponding to a strength of 4 mm was observed. To reduce test error, three samples were prepared for each blended ratio of the above tests, and the average value of the three specimens was used for data analysis.

The cubic sticks measuring approximately 1 cm × 1 cm × 2 cm (length × width × height) were trimmed from the central portion of the CSL sample prior to microstructural testing. Before scanning, the soil sticks were slightly broken at a height of approximately 1 cm and the new surface was used to examine the microstructure of the sample. Then, without disturbing the fracture surface, the stick halves were glued to the shooting pad with an electron-conductive tape and the platinum (Pt) coating was sputtered in a sputtering ion apparatus. An MLA 630F SEM was applied to record the microstructure photos of all samples. In order to quantify the microstructural evolution, this study used IPP software for image processing. There has been a lot of literatures providing an introduction on IPP software (see, e.g., the

works of Xu et al. [31], Liu et al. [33], amongst others). In this study the pore size, area, shape, and angle were analyzed, where the size, area, and angle can be obtained directly from the software, and the shape was represented by the short diameter to long diameter ratio. The value of the short diameter to long diameter ratio (C) varies between 0 and 1. It can be obtained by Eq. (1).

$$C = \frac{B}{L} \tag{1}$$

where L is the long axis length of the pore and B is the short axis width of the pore. A large value of C indicated that length was like the width of the loess pore, and the sharp of loess pore tended to be round or square in-plane, while a small value C illustrated a great gap between length and width and the loess pore inclined to the rectangular or oval shape [40].

3 Results and Discussions

3.1 Specific Gravity

The specific gravity of soil is one of the basic physical properties and is the main indicator for calculating pore ratios and evaluating soil types. Fig. 2 shows the variation of the specific gravity of the CSL samples with the amount of cement blended. The specific gravity of the CSL samples increases from the initial values (Table 1) by 0.48%, 0.74%, 1.04%, and 1.26%, with cement additions of 2%, 4%, 6%, and 8%, respectively. The specific gravity of the CSL sample increases with the amount of cement blended. However, the magnitude of change is not significant. The specific gravity depends on the structure of the loess, its mineral composition, and organic matter content. The specific gravity decreases as the organic matter content increases and increases as the mineral content increases [32]. Due to the rich mineral content of the cement, the proportion of mineral components increases when mixed into the loess, resulting in an increase in the specific gravity of CSL samples. The specific gravity of the loess particles is directly related to the type of elements contained in the soil, and only part of the improved loess reacts chemically with the cement particles to produce new substances [33]. In addition, a significant part of the loess particles does not participate in the reaction, and the reaction only occurs between the particles of ion exchange, chemistry, and other reactions, no new elements are generated, so the specific gravity of the soil particles does not change greatly [41]. The results of this test were also confirmed by Ghadakpour et al. [22], who found that the specific gravity of the cement was greater than loess, thus causing the specific gravity of the CSL samples to increase as the cement content increased.

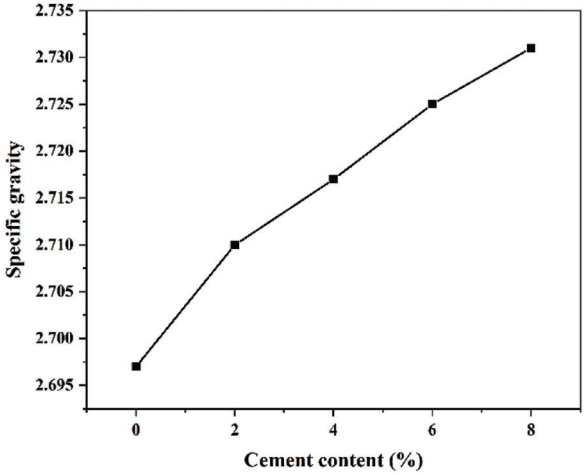

Figure 2: Variation of specific gravity with cement content

3.2 Consistency Limit

The Liquid Limit (LL) and Plastic Limit (PL) are the consistency limit for variations in the physical state of the loess and mainly reflect the degree of interaction between loess particles and water. Loess is highly water-sensitive, and the measurement of the LL, PL, and plasticity index of loess can effectively determine the degree of water binding and stability of the loess under different water content conditions, thus indirectly reflecting the engineering properties of the loess [42]. The plasticity index is one of the most important physical indicators of clay, which integrally reflects the material composition of clay and is widely used in the classification and evaluation of soils [43]. Furthermore, the plasticity index also can reflect the influence of soil mineral composition and particle size. As the cement content increases, the LL decreases, the PL shows an increase followed by a decrease, and the plastic limit index decreases followed by an increase (Fig. 3). When cement is added to the loess, strong interaction between the loess and the cement particles occurs, which will form cementations material and fill the macropores in the loess. Metelková et al. [44] found that the liquid limit increases with the number of macropores. Thus, the liquid limit decreases as the cement content increases. The plastic limit of the loess is proportional to the size of the aggregates [45]. The production of cementing material acts as a connection between the aggregates, resulting in larger aggregate sizes in the CSL samples. However, when the cement content is increased further, the reaction between the particles cannot proceed further and this leads to a slight decrease in the plastic limit. The addition of cement still has a filling effect on the pores and the liquid limit still shows a decreasing trend. In general, the greater the plastic limit of the soil, the stronger is the pressure resistance and poorer is the permeability of the soil [13]. Therefore, the addition of cement has a beneficial effect on the compression strength of the loess. Kang et al. [46] have similar findings on the liquid and plastic limits of CSL samples. Zhi et al. [47] also tested the consistency limit of 1:9 and 1:6 CSL samples, and found that as the cement content increased the liquid limit decreased and the plastic limit increased.

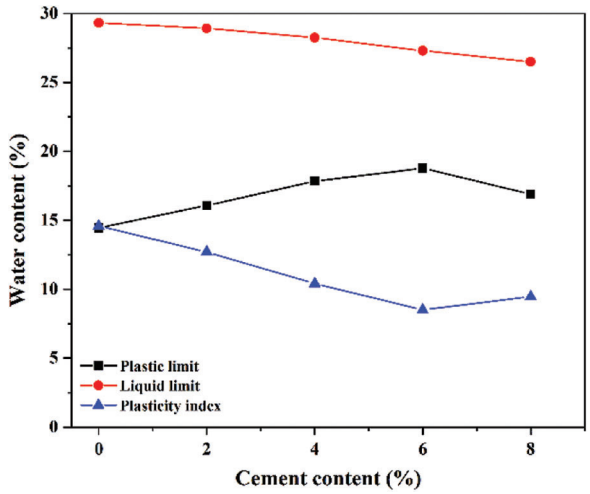

Figure 3: Relationship between consistency limit and cement content

3.3 Compacted Test

Fig. 4 presents the correlation between dry density and water content, and the compaction coefficient of 95% of the maximum dry density can be obtained. As the cement percentage increased from 0% to 8%, the maximum dry density of the CSL samples decreased from the initial values (cement content 0%) by 1.85%, 3.70%, 4.59%, and 7.40%, respectively. while an increase of about 0.66%, 2.19%, 2.68%, and 4.37% is obtained for the optimum water content. Compared to the compaction curve of the compacted loess

(cement content 0%), the peak area of the compaction curve of the CSL sample is gentler than the compacted loess, which displays that the dry density of the CSL sample is less sensitive to water content than compacted loess [48]. These changes may be related to pozzolanic reactions in relation to the associated clay material [49]. Optimal water content also increases with increasing content if the loess is improved with other stabilizers [50,51]. Meanwhile, Ghadakpour et al. [22] obtained similar trends to this study for the maximum dry density and optimum water content of the CSL samples.

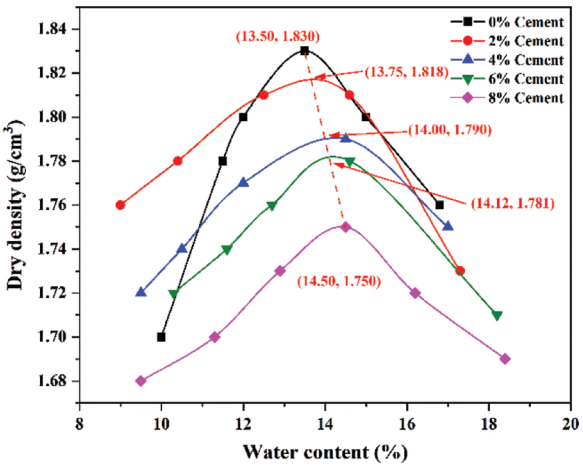

Figure 4: Cement improved effect on the compaction test results

3.4 Unconfined Compression Test

The UCS is the maximum axial stress that a specimen can be subjected to without any lateral restriction and is widely used because of its ease of testing and its ability to quickly reflect the strength characteristics of the specimen. Fig. 5a shows the UCS increases with increasing cement content and curing times. The unconfined compression strength of CSL samples increases non-linearly with increasing cement content at different curing times [21]. For CSL samples with a content of 8%, the unconfined compression strength reach 873.5, 1146.7, and 1993.3 kPa at 7 days, 14 days, and 28 days of curing, respectively, which is approximately 3.7, 4.9, and 8.5 times higher than initial values (cement content 0%), indicating a significant increase in compression strength. The curve of UCS and cement content can be fitted using the equation, $y = a - b \times c^x$, and the obtained fitted curve of UCS and the corresponding fitted parameters are indicated in Fig. 5b and Table 3, respectively. It can be noticed that the Asymptotic model fits well between the USC and the cement content, all of which are above 0.98. As the cement content increases, the UCS gradually increases, but the growth rate gradually decreases. When the cement content is greater than 2%, the growth rate of UCS decreases significantly. This is because the rapid carbonation of cement with water and carbonates in the loess when the cement content is low (<2%), results in flocculation of the soil particles and an increase in the contact surface between larger particles, thus increasing the bonding and compression strength of the loess structure [20]. This result is consistent with the research results of Cui et al. [52] and Liu et al. [33].

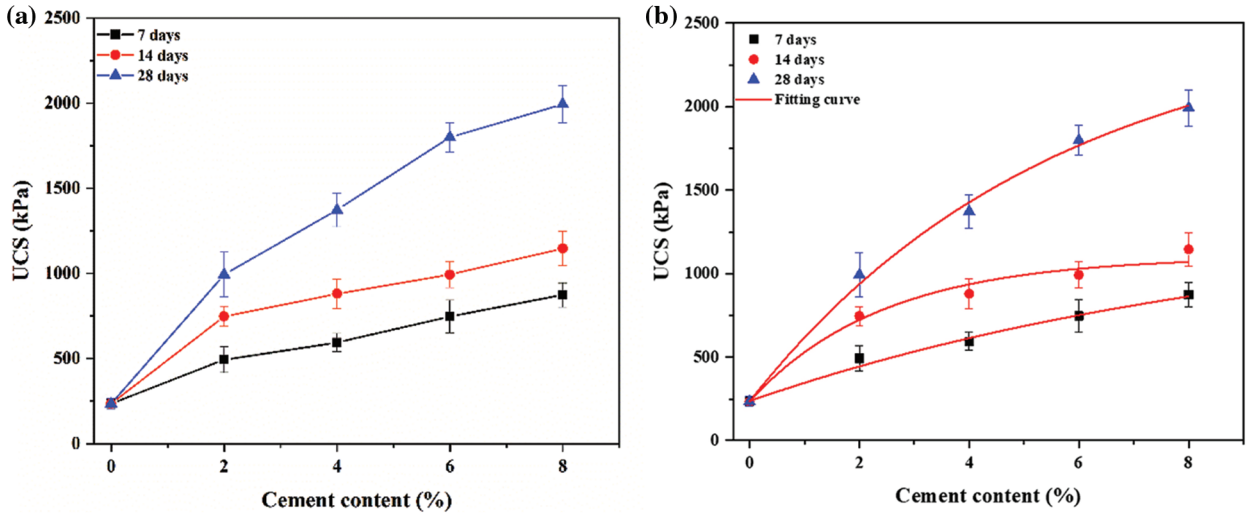

Figure 5: (a) Variation of UCS with cement content; (b) Fitting curve of UCS

Table 3: The fitting equation for UCS to cement content

Curing time/day	Fitting equation	R^2
7	$q_u = 1101.5 - 865.1 \times 0.66^c$	0.986
14	$q_u = 1356.4 - 1118.8 \times 0.90^c$	0.988
28	$q_u = 2554.9 - 2319.3 \times 0.84^c$	0.997

Note: q_u is USC; c is the cement content.

3.5 Shear Strength Parameters

The purpose of the direct shear test is to determine the values of the shear strength parameter. Fig. 6 shows the change in cohesion and internal friction angle of CSL after 7 days of curing time. The variations of cohesion exhibited a continuously increasing trend with an increase in cement content. The contribution of cement to cohesion and the internal friction angle is significant. As the cement percentage increase from 0% to 8%, the cohesion of the CSL samples increase from the initial values (cement content 0%) by 171.9%, 182.2%, 206.5%, and 223.4%, respectively. Meanwhile, an increase of about 78.6%, 86.6%, 97.1%, and 104.7% is obtained for the internal friction angle. It is because the hydration reaction of the stabilizer, the hydration products increase, which makes the average particle diameter increase, and the contact area between the particles increases, and then the cohesion increases [53]. Meanwhile, as the pozzolanic reaction proceeds of CSL samples further, gels material is generated which adheres to the surface of the particles, thus changing the surface roughness and arrangement of the particles, which increases the internal friction angle between the particles [54]. As the cement content increases, the rate of increase in cohesion and internal friction angle decreases. The most significant increase in cohesion and internal friction angle occurs when the cement content increases from 0% to 2%. When the cement content is greater than 2%, the growth rate gradually slows down, and the results correspond to the UCS. Interestingly, these findings do not only apply to loess, Ghadakpour et al. [22] tested the shear strength parameters of clay and loess with the addition of cement and both discovered this result.

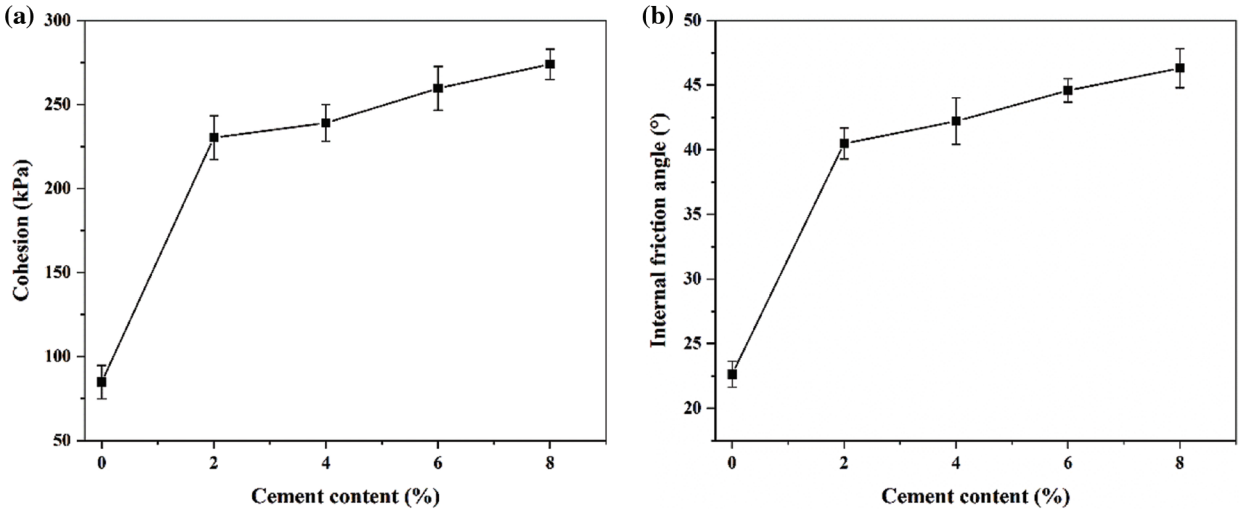

Figure 6: Relationship between shear strength parameters and cement content

3.6 Microstructure of CSL Samples

3.6.1 Morphological of CSL Samples

The fabric resulting from compacted loess (cement content 0%) and CSL samples (cement content 8% and curing time 28 days) are investigated with SEM observations, which exhibit differential aggregations of loess particles (Fig. 7). Fig. 7a illustrates the morphology of the compacted loess surface. Close examination of the images in Fig. 7a reveals that clay and silt particles are often correlated together to form aggregates [55]. Moreover, the arrangement between the structures is relatively loose with obvious inter-aggregate pores. Fig. 7b shows the surface morphology of the CSL sample. Fig. 7c is a magnified view of the box in Fig. 7b. Compared to compacted loess, the surface of the CSL sample is more irregular than compacted loess [33]. And due to the addition of cement, physical and chemical reactions with the loess produced C-S-H gel and ettringites. Ettringites crosslink to form a framework and C-S-H gels form a network to wrap the loess particles and other materials [56]. Both hydration products enhance the strength of the loess samples.

3.6.2 Pore Size Distribution

Fig. 8 provides an insight into the area variation of the different pore types. Compared to compacted loess, the pore area of CSL samples is significantly reduced. According to the literature [57,58], the pores in all loess samples were classified into four different grades based on the diameters, with micropores ranging from 0 to 2 μm, small pores from 2 to 8 μm, mesopores from 8 to 32 μm and macropores greater than 32 μm. Table 4 demonstrates the proportion of the number of different pore sizes to the total number of pore sizes for the compacted loess and CSL sample. In both compacted loess and CSL samples, small pores and mesopores make up the major component of the number of total pores, accounting for approximately 90%, and this is similar to the results for Liu et al. [33]. After the addition of cement, the proportion of micro and small pores in the sample increases, and the proportion of mesopores and macropores decreases. At the same time, the average pore diameter and average pore area decrease from 12.44 and 229.04 to 8.72 and 84.68 μm^2, a reduction of 29.9% and 63.0%, respectively. It shows the physicochemical reactions will occur after adding cement, and the loess structure will be changed.

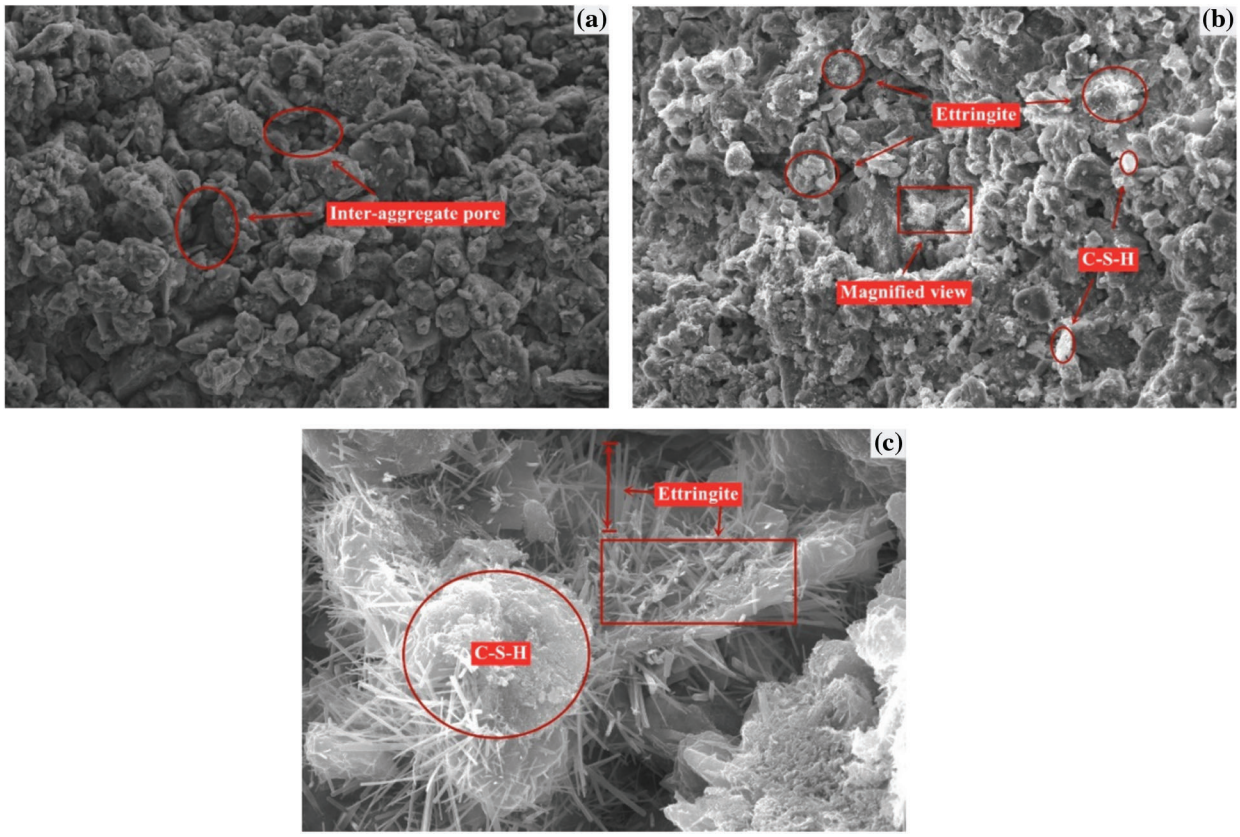

Figure 7: SEM images of compacted loess and CSL samples (a: compacted loess; b: CSL sample; c: magnified view of box in b)

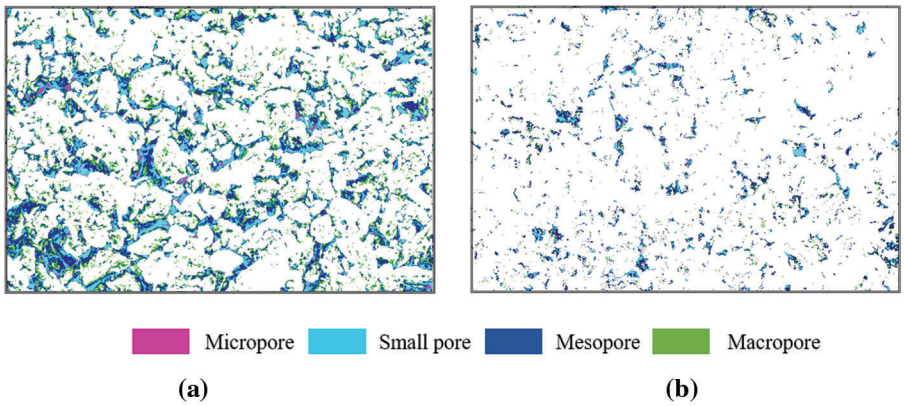

Figure 8: Pore size distribution (a: compacted loess; b: CSL sample)

Table 4: The proportion of total area occupied by different pore sizes

Sample	≤2 μm (%)	2–8 μm (%)	8–32 μm (%)	≥32 μm (%)	Average pore size (μm)	Average pore area (μm^2)
Compacted loess	5.79	48.30	37.23	7.34	12.44	229.04
CSL sample	7.34	57.07	34.24	1.36	8.72	84.68

3.6.3 Pore Shape Distribution

The pore shape distribution in the compacted loess and CSL samples is illustrated in Fig. 9. The pore shape of both the compacted loess and CSL samples is taken to a maximum in the range of 0.4 to 0.6. When the short diameter to long diameter ratio is less than 0.6, the ratio of compacted loess pores is smaller than that of the CSL samples, while the short diameter to long diameter ratio is larger than 0.6, the result is the opposite. Therefore, the addition of cement tends to flatten the pores, thus enhancing the structural strength of the loess. The short diameter to long diameter ratio of cement loess was also tested by Sun et al. [32], and provided similar results to this study. However, these results do not suitable for all stabilizers, as Wang et al. [59] and Liu et al. [60] analyzed the pore shape factors for lignin and microbial stabilized loess respectively, and found that the variation in pore shape was not consistent with this study.

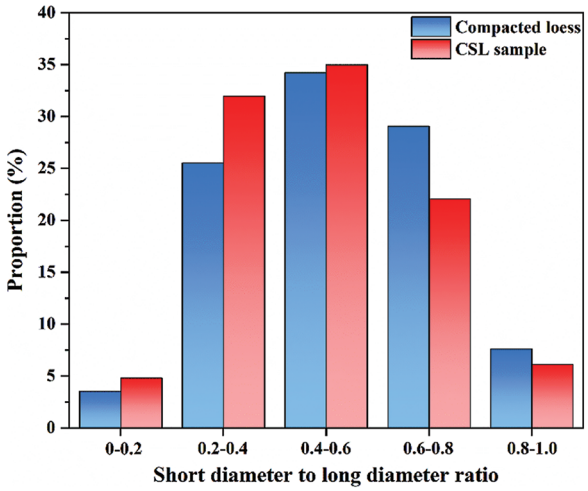

Figure 9: Pore shape distribution

3.6.4 Pore Angle Distribution

The pore angle distribution, an indicator to characterize the orientation of the pores, is introduced into this study to evaluate the orientation microstructure of the loess [39,61]. It is the angle between the long axis of the pore in the plane and the x-axis, and by the magnitude of the angle, it reflects the ordering of the pores in space [62,63]. As can be seen from Fig. 10, the angle distribution of pores is relatively average for both the compacted loess and CSL sample, with no significant sudden changes. When pore angles between 20° and 40°, the compacted loess is significantly higher than the CSL samples, while at pore angles of 140° to 160° the proportion of CSL samples is greater than that of the compacted loess. The distribution of the other pore angles in the compacted loess and CSL samples is essentially the same in proportion. Therefore, the pore angle is not significantly changed by the addition of cement. This result is consistent with the research results of Yi et al. [41].

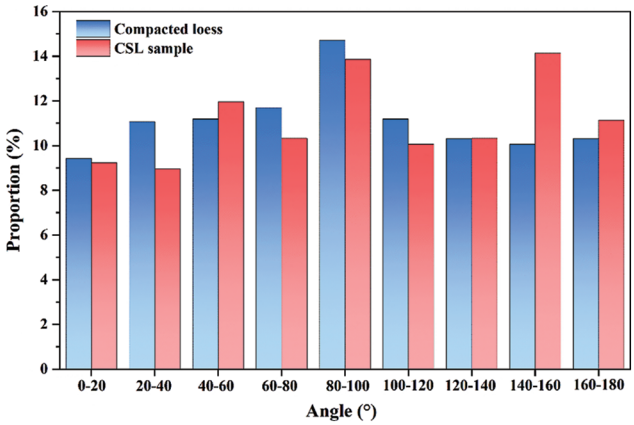

Figure 10: Pore angle distribution

3.7 Mechanism of Cement Stabilization

Cement is a water-hardened inorganic cementitious material that hardens in air or water. The formation of the CSL samples is mainly due to the cementation of the calcium and aluminum hydrates with each other, which lowers the liquid limit and changes the soil structure, increasing the shear strength. CSL samples have both physical and chemical reactions in the formation process, the main effects include ion exchange, pozzolanic reaction, carbonation, cementation, and crystallization. It can be expressed by the following chemical reaction equation [64,65]:

$$CaSiO_2 + H_2O \rightarrow CaOSiO_2 \cdot yH_2O + Ca(OH)_2 \tag{2}$$

$$CO_2 + H_2O \rightarrow H_2CO_3 \tag{3}$$

$$Ca(OH)_2 + H_2CO_3 \rightarrow CaCO_3 + H_2O \tag{4}$$

$$CaSiO_3 + H_2CO_3 \rightarrow CaCO_3 + SiO_2 + H_2O \tag{5}$$

After cement and loess are mixed uniformly and deionized water is added, physicochemical reactions such as ion exchange, pozzolanic reaction, and carbonization and crystallization will take place in CSL samples. The ion exchange decreases the electric potential in the double electric layer, thins the diffusion layer, and increases the van der Waals forces between the soil particles. The pozzolanic reaction will produce gel substances, and the carbonization of cement will convert to calcium carbonate [66]. The crystallization reaction is the change of $Ca(OH)_2$ from an amorphous state to a crystalline state. During the structure formation of CSL samples, the Ca^{2+} and OH^- are ionized from cement after hydration reaction. The hydration of cement is a thermodynamic reaction and provides an alkaline environment for the formation of the CSL sample structure, accompanied by the generation of heat of hydration, which facilitates the reaction [54]. Ca^{2+} reacts with active SiO_2 and Al_2O_3 in the CSL sample in pozzolanic reaction to form ettringite and C-S-H gels (Fig. 7c) [67]. They have a connecting effect of loess structure and will fill the pores between the particles, a result that has been verified in Section 3.6.2. This is due to the presence of large amounts of $Ca(OH)_2$ and Ca^{2+} and OH^- in the gel substances, and exchange with the metal ions adsorbed on the surface of the loess particles, causing the loess particles to form larger aggregates, which combine to form a chain-like structure of CSL sample particles, thus reducing the volume of inter-aggregates pores and making loess structure denser, thus increasing the strength. As the hydration reaction continues, $Ca(OH)_2$ gradually increases and reacts with the CO_2 in the air to produce $CaCO_3$, which enhances the cementation strength between the loess structures. With the cementation strength increasing, a traction is generated on the aggregates, which not only causes a change in the

length of the long diameter but also in the short diameter to long diameter ratio of the pore. The results of Section 3.6.3 reveal that with the addition of cement the short diameter to long diameter ratio of pores increases in the range 0–0.4 and decrease in the range 0.6–1.0, so demonstrating that the generation of traction tends to flatten off the pore shape. This also has an enhancing effect on the strength of the loess structure, as the loess is mainly affected by the pores that have larger values of the short diameter to long diameter ratio during the process of compression [33]. The pozzolanic reaction of cement produces ettringite and C-S-H gels, which have an enhancing effect on the strength of the loess structure and cause traction between the particles to change the size and shape of the pores, working together with $Ca(OH)_2$ to build the framework for CSL samples [59]. A description of the physicochemical reactions that occur in the loess after the addition of cement using PowerPoint software is shown in Fig. 11.

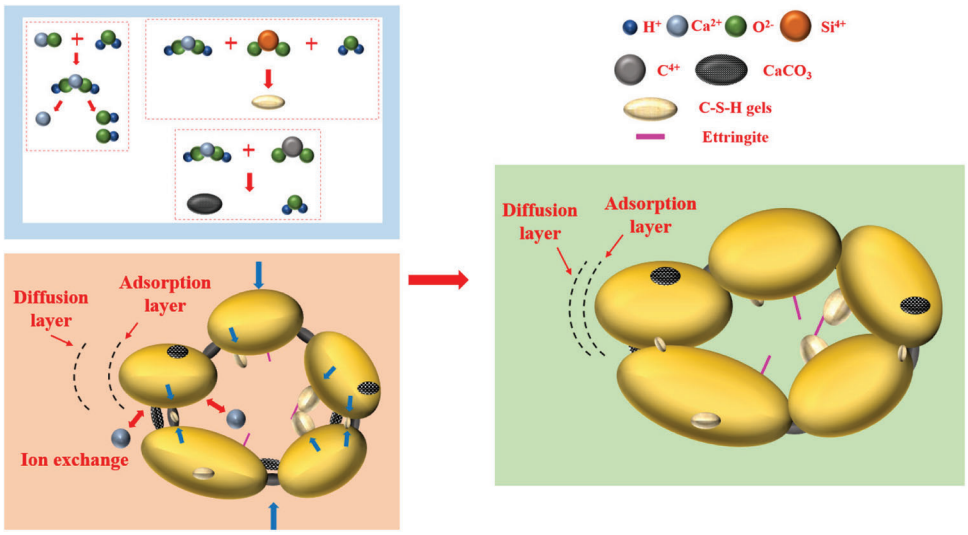

Figure 11: A schematic diagram of the formation of the CSL sample structure

4 Conclusions

In this study, the main physical and mechanical properties of CSL samples with different cement content were investigated, and the change reasons were explored by the mean SEM test. The conclusions were summarized as follows:

1. With the addition of cement, the main physical properties of the CSL samples were changed. The specific gravity and optimum water content increased and the liquid limit and maximum dry density decreased. However, the plastic limit showed an increase followed by a decrease, and the plasticity index decreased followed by an increase. The reasons for the changes are all related to the physicochemical reactions between the cement and the loess particles.
2. The UCS and shear strengths of the CSL samples increased with increasing cement content. For the same curing time, the USC and cement content was better fitted using the Asymptotic model. The UCS and shear strength parameters grew faster when the cement content was less than 2%, however, the growth rate decreased when the cement content was larger than 2%. Therefore, a cement content of 2% was a great choice for the construction process provided that the construction requirements were satisfied.
3. The results of SEM showed that the structure of the CSL samples was denser and had no obvious inter-aggregate pores. Meanwhile, compared to compacted loess, produced C-S-H gel and ettringite.

4. IPP software was used for quantitative analysis to compacted loess and CSL samples pores. Compared to compacted loess, the CSL sample showed an increase in the proportion of micro and small pores and a decrease in the proportion of mesopores and macropores. The pore shape had a tendency to flatten, but there was basically no effect on the pore angle distribution.
5. In the process of structure formation of CSL samples, the pozzolanic reaction of the cement produces ettringite and C-S-H gels, which had an enhancing effect on the structural strength of the loess, and the traction between the particles changed the size and shape of the pores, which together with Ca $(OH)_2$ built the framework of the CSL sample.

Author Contributions: Kui Liu and Kangze Yuan designed research; Kui Liu, Bowen Yang, and Guoyang Yi performed all experiments and analyzed the data. Kangze Yuan calculated the surface area and gave suggestions. Kangze Yuan wrote the paper. All authors read and approved the final manuscript.

Data Availability: The data used to support the findings of this study are available from the corresponding author upon request.

Acknowledgement: We thank research staffs for their contributions to this work.

Funding Statement: This study was supported by the key research and development program of Shaanxi Province in the form of grants awarded to KL (Grant No. 2017ZDXM-SF-087), and BWY (Grant No. 2020SF-436). The funders had no role in study design, data collection and analysis, decision to publish, or preparation of the manuscript.

Conflicts of Interest: The authors declare that they have no conflicts of interest to report regarding the present study.

References

1. Yu, B., Liu, G., Liu, Q., Li, H., Zhao, Z. H. (2019). Seasonal variation of deep soil moisture under different land uses on the semi-arid Loess Plateau of China. *Journal of Soils and Sediments, 19,* 1179–1189. DOI 10.1007/s11368-018-2119-8.
2. Wang, J. D., Li, P., Ma, Y., Wang, X. G. (2020). Change in pore-size distribution of collapsible loess due to loading and inundating. *Acta Geotechnica, 15,* 1081–1094. DOI 10.1007/s11440-019-00815-9.
3. Rost, K. T. (2001). Late Holocene loess deposits and dust accumulation in the alpine meadow belt of the Wutai Shan, China. *Quaternary International, 76,* 85–92. DOI 10.1016/S1040-6182(00)00092-6.
4. Pye, K. (1995). The nature, origin and accumulation of loess. *Quaternary Science Reviews, 14,* 653–667. DOI 10.1016/0277-3791(95)00047-X.
5. Smalley, I., Rogers, C. (1996). Loess: The yellow earth. *Geology Today, 12,* 186–193. DOI 10.1046/j.1365-2451.1996.00015.x.
6. Rollins, K. M., Rogers, G. W. (1994). Mitigation measures for small structures on collapsible alluvial soils. *Journal of Geotechnical Engineering, 120,* 1533–1553. DOI 10.1061/(ASCE)0733-9410(1994)120:9(1533).
7. Leng, Y. Q., Peng, J. B., Wang, Q. Y., Meng, Z. J., Huang, W. L. (2018). A fluidized landslide occurred in the Loess Plateau: A study on loess landslide in South Jingyang tableland. *Engineering Geology, 236,* 129–136. DOI 10.1016/j.enggeo.2017.05.006.
8. Zhang, Y. G., Tang, J., Liao, R. P., Zhang, M. F., Zhang, Y. (2021). Application of an enhanced BP neural network model with water cycle algorithm on landslide prediction. *Stochastic Environmental Research and Risk Assessment, 35,* 1273–1291. DOI 10.1007/s00477-020-01920-y.
9. Zhang, Y. G., Tang, J., He, Z. Y., Tan, J. K., Li, C. (2021). A novel displacement prediction method using gated recurrent unit model with time series analysis in the erdaohe landslide. *Natural Hazards, 105,* 783–813. DOI 10.1007/s11069-020-04337-6.

10. Peng, J. B., Wang, G. H., Wang, Q. Y., Zhang, F. Y. (2017). Shear wave velocity imaging of landslide debris deposited on an erodible bed and possible movement mechanism for a loess landslide in Jingyang, Xi'an, China. *Landslides, 14,* 1503–1512. DOI 10.1007/s10346-017-0827-6.
11. Zhuang, J. Q., Peng, J. B., Wang, G. H., Wang, Y. (2018). Distribution and characteristics of landslide in Loess Plateau: A case study in Shaanxi Province. *Engineering Geology, 236,* 89–96. DOI 10.1016/j.enggeo.2017.03.001.
12. Torabi, A. M., Taherabadi, E. (2018). Modification of silty clay strength in cold region's pavement using glass residue. *Cold Regions Science and Technology, 154,* 111–119. DOI 10.1016/j.coldregions.2018.06.005.
13. Zhao, Y., Zhuang, J. Q., Wang, Y., Jia, Y. J., Niu, P. Y. (2020). Improvement of loess characteristics using sodium alginate. *Bulletin of Engineering Geology and the Environment, 79,* 1879–1891. DOI 10.1007/s10064-019-01675-z.
14. Iranpour, B., Haddad, A. (2016). The influence of nanomaterials on collapsible soil treatment. *Engineering Geology, 205,* 40–53. DOI 10.1016/j.enggeo.2016.02.015.
15. Choobbasti, A. J., Samakoosh, M. A., Kutanaei, S. S. (2019). Mechanical properties soil stabilized with nano calcium carbonate and reinforced with carpet waste fibers. *Construction and Building Materials, 211,* 1094–1104. DOI 10.1016/j.conbuildmat.2019.03.306.
16. Gao, L., Ren, K., Ren, Z., Yu, X. (2018). Study on the shear property of nano-MgO-modified soil. *Marine Georesources & Geotechnology, 36,* 465–470. DOI 10.1080/1064119X.2017.1335813.
17. Jia, L., Li, C. X., Guo, J. (2020). Mechanical properties of lime-fly ash-sulphate aluminum cement stabilized loess. *Journal of Renewable Materials, 8(10),* 1357–1373. DOI 10.32604/jrm.2020.012136.
18. Tang, C. S., Shi, B., Zhao, L. Z. (2010). Interfacial shear strength of fiber reinforced soil. *Geotextiles and Geomembranes, 28,* 54–62. DOI 10.1016/j.geotexmem.2009.10.001.
19. Gao, Z. G., Zhang, X. M., Wang, Q., Su, Y. Q., Wang, J. (2022). The influence of freeze-thaw cycles on unconfined compressive strength of lignin fiber-reinforced loess. *Journal of Renewable Materials, 10,* 4. DOI 10.32604/jrm.2022.017374.
20. Su, X. P. (2014). Research on the properties of collapsible loess reinforced by cement. *Advanced Materials Research, 1015,* 110–113. DOI 10.4028/www.scientific.net/AMR.1015.110.
21. Zhang, C., Jiang, G., Su, L., Zhou, G. (2017). Effect of cement on the stabilization of loess. *Journal of Mountain Science, 14,* 2325–2336. DOI 10.1007/s11629-017-4365-4.
22. Ghadakpour, M., Choobbasti, A. J., Kutanaei, S. S. (2020). Experimental study of impact of cement treatment on the shear behavior of loess and clay. *Arabian Journal of Geosciences, 13,* 184. DOI 10.1007/s12517-020-5181-7.
23. Wang, J. D., Peng, S. J., Xie, W. L. (2013). Study on the cement-improved loess under the vibratory load by dynamic tests. *Advanced Materials Research, 838–841,* 1302–1308. DOI 10.4028/www.scientific.net/AMR.838-841.1302.
24. Liu, J., Wang, T., Tian, Y. (2010). Experimental study of the dynamic properties of cement-and lime-modified clay soils subjected to freeze–thaw cycles. *Cold Regions Science and Technology, 61,* 29–33. DOI 10.1016/j.coldregions.2010.01.002.
25. Jiang, Y., Ni, C., Sha, H. (2021). Deterioration characteristics of cement-improved loess under dry–wet and freeze–thaw cycles. *PLoS One, 16,* 199. DOI 10.1371/journal.pone.0253199.
26. Yuan, K. Z., Ni, W., Lü, X. F. (2020). Collapse behavior and microstructural change of loess under different wetting-drying cycles. *IOP Conference Series: Earth and Environmental Science, 598,* 012036. DOI 10.1088/1755-1315/598/1/012036.
27. Li, P., Vanapalli, S., Li, T. (2016). Review of collapse triggering mechanism of collapsible soils due to wetting. *Journal of Rock Mechanics and Geotechnical Engineering, 8,* 256–274. DOI 10.1016/j.jrmge.2015.12.002.
28. Lyu, L., Li, D., Chen, Y. (2021). Dynamic chemistry based self-healing of asphalt modified by diselenide-crosslinked polyurethane elastomer. *Construction and Building Materials, 293,* 123480. DOI 10.1016/j.conbuildmat.2021.123480.
29. Vos, K., Vandenberghe, N., Elsen, J. (2014). Surface textural analysis of quartz grains by scanning electron microscopy (SEM): From sample preparation to environmental interpretation. *Earth-Science Reviews, 128,* 93–104. DOI 10.1016/j.earscirev.2013.10.013.

30. Gao, G. (1981). Classification of microstructures of loess in China and their collapsibility. *Science China (Serial A), 24 (7),* 962–974.
31. Xu, P., Zhang, Q., Qian, H. (2021). Microstructure and permeability evolution of remolded loess with different dry densities under saturated seepage. *Engineering Geology, 282,* 105875. DOI 10.1016/j.enggeo.2020.105875.
32. Sun, G., Zhang, J., Dang, Y., Ding, C. (2019). Microstructure and strength features of warm and ice-rich frozen soil treated with high-performance cements. *Journal of Mountain Science, 16,* 1470–1482. DOI 10.1007/s11629-018-5197-6.
33. Liu, H. M., Wang, L. M., Gao, P. (2014). The mechanical properties of cement reinforced loess and pore microstructure characteristics. *Applied Mechanics and Materials, 527,* 25–30. DOI 10.4028/www.scientific.net/AMM.527.25.
34. ASTM (2006). *Annual book of ASTM standards*. West Conshohocken, PA: ASTM International.
35. ASTM (2007). *Designation D854-06, standard test method for specific gravity of soil solids by water pycnometer: Annual book of ASTM standards*. West Conshohocken, PA: ASTM.
36. Li, J. Q., Zhang, X. D., Zou, M., Li, H. (2012). Soil liquid limit and plastic limit treating system based on analytic method. *Procedia Earth and Planetary Science, 5,* 175–179. DOI 10.1016/j.proeps.2012.01.031.
37. ASTM. ASTM standard D2487 (2011). *Standard practice for classification of soils for engineering purposes (Unified soil classification system)*, vol. 18. West Conshohocken, PA, USA: American Society for Testing Materials.
38. ASTM. ASTM standard D 2166 (2000). *Standard practice for unconfined compressive strength of cohesive soil*, vol. 9. West Conshohocken, PA. American Society for Testing and Materials.
39. Cheng, W. C., Xue, Z. F., Wang, L., Xu, J. (2019). Using post-harvest waste to improve shearing behaviour of loess and its validation by multiscale direct shear tests. *Applied Sciences, 9,* 5206. DOI 10.3390/app9235206.
40. Ni, W. K., Yuan, K. Z., Lü, X. F., Yuan, Z. H. (2020). Comparison and quantitative analysis of microstructure parameters between original loess and remoulded loess under different wetting-drying cycles. *Scientific Reports, 10,* 5547. DOI 10.1038/s41598-020-62571-1.
41. Yi, Z. H., Zhang, J. M., Zhang, H., Wang, H. L. (2021). Microcosmic pore characteristics evolution of the cement improved frozen soil after thawing compression. *Hydrogeology & Engineering Geology, 48,* 4. DOI 10.16030/j.cnki.issn.1000-3665.202007037.
42. Yan, C., Wan, Q., Xu, Y. (2018). Experimental study of barrier effect on moisture movement and mechanical behaviors of loess soil. *Engineering Geology, 240,* 1–9. DOI 10.1016/j.enggeo.2018.04.007.
43. Petry, T. M., Das, B. (2001). Evaluation of chemical modifiers and stabilizers for chemically active soils—Clays. *Transportation Research Record, 1757*. 43–49. DOI 10.3141/1757-05.
44. Metelková, Z., Boháč, J., Přikryl, R., Sedlářová, I. (2012). Maturation of loess treated with variable lime admixture: Pore space textural evolution and related phase changes. *Applied Clay Science, 61,* 37–43. DOI 10.1016/j.clay.2012.03.008.
45. Ma, Y., Chen, W. (2021). Study on the mechanism of stabilizing loess with lime: Analysis of mineral and microstructure evolution. *Advances in Civil Engineering, 2021,* 1–11. DOI 10.1155/2021/6641496.
46. Kang, G., Tsuchida, T., Tang, T. X., Kalim, T. P. (2017). Consistency measurement of cement-treated marine clay using fall cone test and casagrande liquid limit test. *Soils and Foundations, 57,* 802–814. DOI 10.1016/j.sandf.2017.08.010.
47. Zhi, B., Yang, L., Liu, E. L. (2014). Study on the mechanical properties of lime-cement-treated loess soils. *Applied Mechanics and Materials, 638–640,* 1408–1413. DOI 10.4028/www.scientific.net/AMM.638-640.1408.
48. Lenoir, T., Dubreucq, T., Lambert, T., Killinger, D. (2021). Safety factor calculation of a road structure with cement-modified loess as subgrade. *Transportation Geotechnics, 30,* 100604. DOI 10.1016/j.trgeo.2021.100604.
49. Seco, A., Ramírez, F., Miqueleiz, L., García, B. (2011). Stabilization of expansive soils for use in construction. *Applied Clay Science, 51,* 348–352. DOI 10.1016/j.clay.2010.12.027.
50. Guney, Y., Sari, D., Cetin, M., Tuncan, M. (2007). Impact of cyclic wetting–drying on swelling behavior of lime-stabilized soil. *Building and Environment, 42,* 681–688. DOI 10.1016/j.buildenv.2005.10.035.

51. Kumar, A., Walia, B. S., Bajaj, A. (2007). Influence of fly ash, lime, and polyester fibers on compaction and strength properties of expansive soil. *Journal of Materials in Civil Engineering, 19,* 242–248. DOI 10.1061/(ASCE)0899-1561(2007)19:3(242).
52. Cui, S. L., Huang, S., Han, L., Zhang, Y. R. (2018). A study of the collapsibility and strength property of loess stabilized by cement kiln ash. *Hydrogeology & Engineering Geology, 45,* 4. DOI 10.16030/j.cnki.issn.1000-3665.2018.04.11.
53. Yang, S., Liu, W. (2020). Application of image-pro plus in the shear strength and micro-structure of solidified soil mixed with fly ash. *Multimedia Tools and Applications, 79,* 10065–10075. DOI 10.1007/s11042-019-07804-w.
54. Yang, X. W., Qu, Y., Zhou, H. R. (2017). Triaxial test about loess solidified by cement silicon powder. *Journal of Guilin University of Technology, 37,* 4.
55. Guo, Y., Ni, W., Liu, H. (2021). Effects of dry density and water content on compressibility and shear strength of loess. *Geomechanics and Engineering, 24,* 419–430. DOI 10.12989/gae.2021.24.5.419.
56. Gu, K., Chen, B. (2020). Loess stabilization using cement, waste phosphogypsum, fly ash and quicklime for self-compacting rammed earth construction. *Construction and Building Materials, 231,* 117195. DOI 10.1016/j.conbuildmat.2019.117195.
57. Qiu, J., Wang, X., Lai, J. (2018). Response characteristics and preventions for seismic subsidence of loess in Northwest China. *Natural Hazards, 92,* 1909–1935. DOI 10.1007/s11069-018-3272-5.
58. Li, X., Li, L. (2017). Quantification of the pore structures of Malan loess and the effects on loess permeability and environmental significance, Shaanxi Province, China: An experimental study. *Environment Earth Science, 76,* 523. DOI 10.1007/s12665-017-6855-7.
59. Wang, Q., Zhong, X., Ma, H. (2020). Microstructure and reinforcement mechanism of lignin-modified loess. *Journal of Materials in Civil Engineering, 32,* 04020319. DOI 10.1061/(ASCE)MT.1943-5533.0003422.
60. Liu, X., Fan, J., Yu, J., Gao, X. (2021). Solidification of loess using microbial induced carbonate precipitation. *Journal of Mountain Science, 18,* 265–274. DOI 10.1007/s11629-020-6154-8.
61. Delerue, J. F., Perrier, E., Yu, Z. Y., Velde, B. (1999). New algorithms in 3D image analysis and their application to the measurement of a spatialized pore size distribution in soils. *Physics and Chemistry of the Earth, Part A: Solid Earth and Geodesy, 24,* 639–644. DOI 10.1016/S1464-1895(99)00093-9.
62. Wang, L., Wang, Y., Sun, X. G. (2011). Influence of pores on the thermal insulation behavior of thermal barrier coatings prepared by atmospheric plasma spray. *Materials & Design, 32,* 36–47. DOI 10.1016/j.matdes.2010.06.040.
63. Kader, M. A., Brown, A. D., Hazell, P. J. (2020). Geometrical and topological evolution of a closed-cell aluminium foam subject to drop-weight impact: An X-ray tomography study. *International Journal of Impact Engineering, 139,* 103510. DOI 10.1016/j.ijimpeng.2020.103510.
64. Chen, T., Gao, X. (2019). Effect of carbonation curing regime on strength and microstructure of portland cement paste. *Journal of CO_2 Utilization, 34,* 74–86. DOI 10.1016/j.jcou.2019.05.034.
65. Zhang, D., Ghouleh, Z., Shao, Y. (2017). Review on carbonation curing of cement-based materials. *Journal of CO_2 Utilization, 21,* 119–131. DOI 10.1016/j.jcou.2017.07.003.
66. Zhang, Y., Yao, Y., Du, W., Zhou, H. (2021). Experimental study on improvement design of loess curing in engineering environment. *Bulletin of Engineering Geology and the Environment, 80,* 3151–3162. DOI 10.1007/s10064-021-02112-w.
67. Qin, L., Gao, X. (2019). Properties of coal gangue-portland cement mixture with carbonation. *Fuel, 245,* 1–12. DOI 10.1016/j.fuel.2019.02.067.